CdTe Photovoltaic Devices for Solar Cell Applications

by Priyalal Wijewarnasuriya

ARL-RP-0349 **December 2011**

A reprint from the *Solar Asia 2011*, Kandy, Sri Lanka, July 28, 2011.

NOTICES

Disclaimers

Army Research Laboratory
Adelphi, MD 20783-1197

ARL-RP-0349 **December 2011**

CdTe Photovoltaic Devices for Solar Cell Applications

Priyalal Wijewarnasuriya
Sensors and Electron Devices Directorate, ARL

A reprint from the *Solar Asia 2011*, Kandy, Sri Lanka, July 28, 2011

REPORT DOCUMENTATION PAGE	*Form Approved* *OMB No. 0704-0188*

1. REPORT DATE *(DD-MM-YYYY)* December 2011	**2. REPORT TYPE** Reprint	**3. DATES COVERED (From - To)**

4. TITLE AND SUBTITLE CdTe Photovoltaic Devices for Solar Cell Applications	**5a. CONTRACT NUMBER**
	5b. GRANT NUMBER
	5c. PROGRAM ELEMENT NUMBER
6. AUTHOR(S) Priyalal Wijewarnasuriya	**5d. PROJECT NUMBER**
	5e. TASK NUMBER
	5f. WORK UNIT NUMBER
7. PERFORMING ORGANIZATION NAME(S) AND ADDRESS(ES) U.S. Army Research Laboratory ATTN: RDRL-SEE-I 2800 Powder Mill Road Adelphi, MD 20783-1197	**8. PERFORMING ORGANIZATION REPORT NUMBER** ARL-RP-0349
9. SPONSORING/MONITORING AGENCY NAME(S) AND ADDRESS(ES)	**10. SPONSOR/MONITOR'S ACRONYM(S)**
	11. SPONSOR/MONITOR'S REPORT NUMBER(S)

12. DISTRIBUTION/AVAILABILITY STATEMENT

Approved for public release; distribution unlimited.

13. SUPPLEMENTARY NOTES

A reprint from the *Solar Asia 2011,* Kandy, Sri Lanka, July 28, 2011

14. ABSTRACT

Cadmium telluride (CdTe) has been recognized as a promising photovoltaic material for thin-film solar cells because of its near optimum bandgap of ~1.5 eV and high absorption coefficient. The energy gap is near optimum for a single junction solar cell and the high absorption coefficient allows films as thin as 2 µm to absorb more than 98% of the above-bandgap radiation. Cells with efficiencies near 17% have been produced for poly-CdTe materials. By alloying with mercury telluride (HgTe), $Hg_{1-x}Cd_xTe(0 \le x \le 1)$ alloy can be obtained with a bandgap energy that falls between the end points of HgTe (E_g= -0.3 eV) and CdTe (E_g =1.5 eV). Because of its bandgap tunability with the Cd composition, $Hg_{1-x}Cd_xTe$ alloy has evolved to become the most important/versatile material for detector applications over the entire infrared wavelength range and has gained traction in the solar cell community.

15. SUBJECT TERMS

Cd(Hg)Te, Cd(Zn)Te, infrared detectors, solar cells, quantum efficiency, spectral response

16. SECURITY CLASSIFICATION OF:			**17. LIMITATION OF ABSTRACT**	**18. NUMBER OF PAGES**	**19a. NAME OF RESPONSIBLE PERSON** Priyalal Wijewarnasuriya
a. REPORT Unclassified	**b. ABSTRACT** Unclassified	**c. THIS PAGE** Unclassified	UU	14	**19b. TELEPHONE NUMBER** (*Include area code*) (301) 394-0963

Standard Form 298 (Rev. 8/98)
Prescribed by ANSI Std. Z39.18

CdTe Photovoltaic Devices for Solar Cell Applications

Priyalal Wijewarnasuriya*
U.S. Army Research Laboratory
Sensors and Electronic Devices Directorate
2800 Powder Mill Road, Adelphi MD 20783
*** Email:** priyalal.s.wijewarnasuriya.civ@mail.mil **Phone: 301 394 0963**

ABSTRACT

Cadmium telluride (CdTe) has been recognized as a promising photovoltaic material for thin-film solar cells because of its near optimum bandgap of ~1.5 eV and high absorption coefficient. The energy gap is near optimum for a single junction solar cell and the high absorption coefficient allows films as thin as 2 μm to absorb more than 98% of the above-bandgap radiation. Cells with efficiencies near 17% have been produced for poly-CdTe materials. By alloying with mercury telluride (HgTe), $Hg_{1-x}Cd_xTe(0 \leq x \leq 1)$ alloy can be obtained with a bandgap energy that falls between the end points of HgTe (E_g= -0.3 eV) and CdTe (E_g =1.5 eV). Because of its bandgap tunability with the Cd composition, $Hg_{1-x}Cd_xTe$ alloy has evolved to become the most important/versatile material for detector applications over the entire infrared wavelength range and has gained traction in the solar cell community.

Key Words: Cd(Hg)Te, Cd(Zn)Te, infrared detectors, solar cells, quantum efficiency, spectral response

INTRODUCTION

Despite long-term research efforts on CdTe solar cells, measured CdTe solar cells efficiencies remain below theoretical limits. Today, the best CdTe solar cells (AM1.5) have reached an efficiency of 16.7%, compared with the theoretical maximum value of 30% for one junction[1]. This large difference between the measured and predicted poly-CdTe solar efficiency is believed to be due to the poor minority carrier life (< 2 nsec) in the absorber layer[1,2]. There are several approaches that have shown promise for reducing the gap between the measured and theoretical efficiency of CdTe. These include removing recombination centers in the grain boundaries, improving crystal quality, and increasing doping concentrations. However, one of the approaches used to overcome these technical challenges takes advantage of mature single-crystal CdTe and CdZnTe thin films grown on Si substrates by molecular beam epitaxy (MBE)[1]. Si substrates provide advantages in terms of their relatively large area (3- to 12-in diameter is easily available). Despite the large lattice mismatch between Si and CdTe, it has been proven that good-quality CdTe can be grown by MBE on Si substrates with uniform structural and electrical properties[3,4]. A tremendous amount of effort in the infrared (IR) community has been devoted to developing CdTe/Si as a composite substrate for subsequent HgCdTe IR material growth by MBE. Currently, high quality CdTe/Si systems with x-ray rocking curve full width at half maximum (FWHM) values measuring less than 60 arcsec for an 8-μm-thick epilayer have been created[5]. This work has led to the production of state-of-the-art HgCdTe photovoltaic (PV) devices over the entire spectral wavelength region covering near IR (NIR) to long-wave IR (LWIR), including large format arrays, multi-color devices, large area devices, etc., on Si substrates. These devices are used in focal plane arrays (FPAs) for military, remote sensing, space-based, and commercial applications. Diffusion currents dominate the highest performance PV detectors, i.e., generation-recombination in the depletion; tunneling currents are negligible (depending of the temperature of operation) compared to the diffusion currents of these state-of-the-art PV devices. A variety of HgCdTe PV devices have been fabricated including planar, mesa, higher operating temperature (HOT), and multi-color.

This innovation in Si-based MBE II-VI material growth allows for fabrication of single- and multi-junction solar devices made of high quality crystalline CdTe and CdZnTe. Today's cost reduction initiative includes novel cell architectures and high volume/lower cost production methodologies. Significant advances have been made in these areas. With crystalline Si greater than 15% to 18%, cell efficiencies have been obtained with complex, high cost cell architectures[6]. Here, I focus on a crystalline-CdTe material for solar cells application. Presently, very few are exploring this material system[7]. For low-cost cells, high quality crystalline Cd(Zn)Te grown on Sapphire substrates are being explored.

DEVICE STRUCTURE

The choice of solar cell detector architecture determines the type of dark currents that impact the overall efficiency of a solar cell. For modeling purposes of this paper, we used $\underline{P}^+$-on-n double layer heterostructure (DLH) detector architecture[8]. $\underline{P}^+$ indicates a higher bandgap than the CdTe as well as higher p-type doping compared with the absorber n-type layer. Figure 1 is a schematic cross section of the DLH detector architecture. The active layer is n-type with doping levels (N_d) in the range ~low 10^{15} to 10^{17} cm^{-3} and a thickness (t_n) in the range of 2–5 μm for complete absorption. L denotes the diffusion length of holes and S_h denotes the surface recombination velocity at the back interface. The cap layer thickness (t_p) is on the order of 0.3 μm and the doping concentration (N_a) is on the order of 10^{18} cm^{-3}.

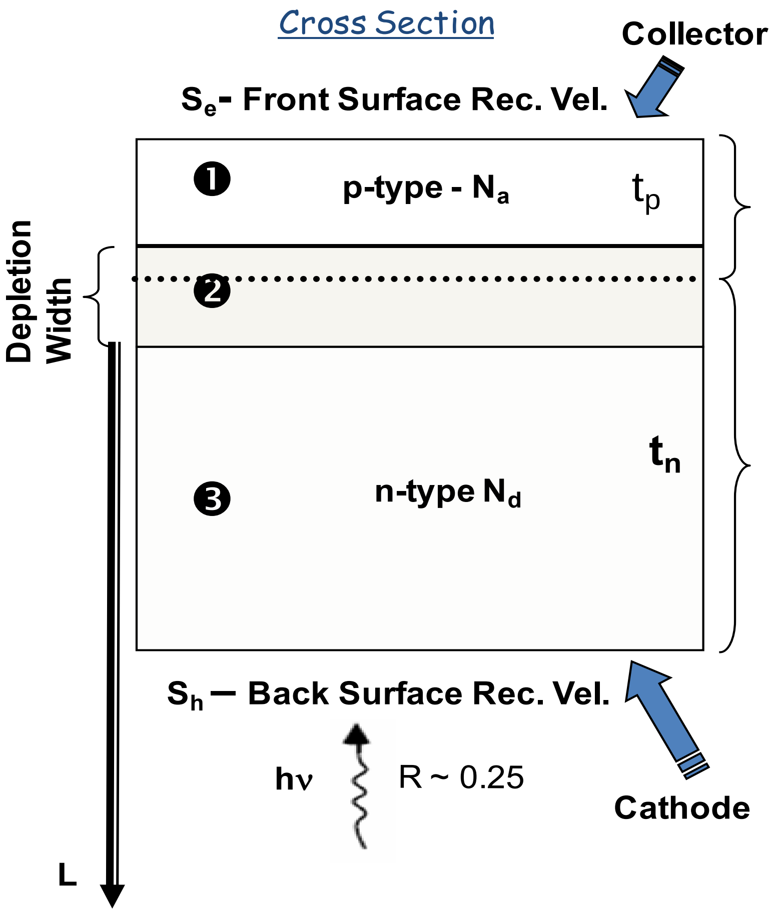

Figure 1. Cross section of a illuminated $\underline{P}^+$-on-n DLH solar cell detector architecture. Illumination is from the CdTe absorber layer side. Reflection loss is 25% and it is neglected in the model calculation. $\underline{P}^+$ indicates higher band gap as well as higher p-type doping than the base n-type layer.

Obtaining high quantum efficiency (QE) requires nearly complete absorption of the incident photons (for all wavelengths) and a high probability that the minority carriers generated are collected at the junction interface presumably through a diffusion process. This implies a high absorption coefficient and a long diffusion length of the minority carriers in the base material. Hence, the requirement is that $t_n > \frac{1}{\alpha(x,\lambda)}$ for the complete absorption and $t_n < L$ for the complete collection of the carriers at the junction. The absorption coefficient α(x,λ,T) at 300 K for CdTe is taken from reference 9. Since the absorption coefficient is higher for shorter wavelength radiation than longer wavelength radiation, shorter wavelength radiation is absorbed closer to the back interface in our device configuration. Therefore, achieving high efficiency devices will require a very low back surface recombination velocity S_h as is discussed in the next section.

QUANTUM EFFICIENCY

Detector QE is defined as the ratio of the number of minority carriers collected by the detector to the number of photons incident on the cell, assuming negligible reflection loses. Under illuminated condition, solar photons passes through the neutral region 3 (QE = QE_h), then through the depletion region 2 (QE = QE_{dep}), and finally through the neutral p-region-1 (QE = QE_e). If all of these regions contribute to the total QE (QE_{total}), then

$$QE_{total} = QE_h + QE_{dep} + QE_e$$

Complete expressions for QE_h, QE_{dep}, and QE_e can be found in ref. 10. A CdTe absorber layer that is too thin results in an incomplete absorption of photons near the bandgap energy and consequently a reduced QE within the spectral band of interest. On the other hand, an absorber layer that is too thick results in decreased QE for photon wavelengths that are absorbed away from the junction since the diffusion length may be shorter than the absorber layer thickness (see Figure 2). Computing QE as a function of thickness for 5 microns and 3.5 microns, the QE is 90% and 95%, respectively, at the shorter wavelength region. This implies that the optimum thickness is 3.5 microns. Back surface recombination velocity should be as low as possible since the high energy photons are absorbing near the back surface. The dash-line in the Figure 2 shows QE versus wavelength for a 10^5 cm/sec recombination velocity. The QE is drastically reduced throughout the entire wavelength band. Similar plots are shown in the Figure 3, which includes QE calculated at 0.3 microns and 0.7 microns versus the back surface recombination velocity. As can be seen, the QE for both wavelengths is approximately 95% up to 10^3 cm/sec, and at high recombination velocities, it falls off drastically. Minority-carrier lifetimes for a variety of epitaxial and thin-film solar-cell materials are given in reference 11. As indicated in the reference, minority-carrier lifetimes $\tau \geq 1$ µs are routinely achieved in both n and p CdTe and 4-µs lifetimes are reported for CdZnTe material as well. It should be noted that for GaInAs and GaInP, lifetimes are less than 10 nsec from the same reference. In this paper, we assume a lifetime value of 150 nsec (lower limit of published results for crystalline n-type CdTe). As indicated in Figure 3, the diffusion length obtained is 9 microns assuming 150 nsec for lifetime, hole mobility of 200 cm^2/Vs in n-type and doping density of 10^{17} cm^{-3}.

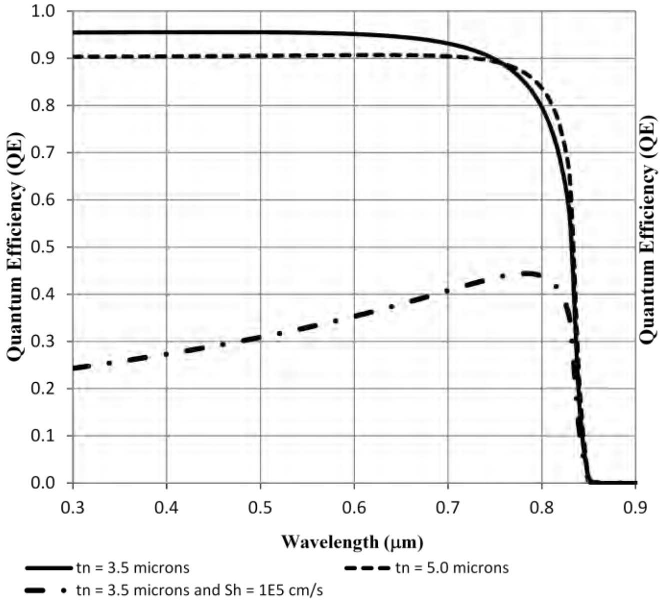

Figure 2. Dependence of quantum efficiency (QE) versus wavelength under different CdTe thickness and 10^5 cm/sec back surface velocity. 10 microns of hole diffusion length was assumed in the calculation.

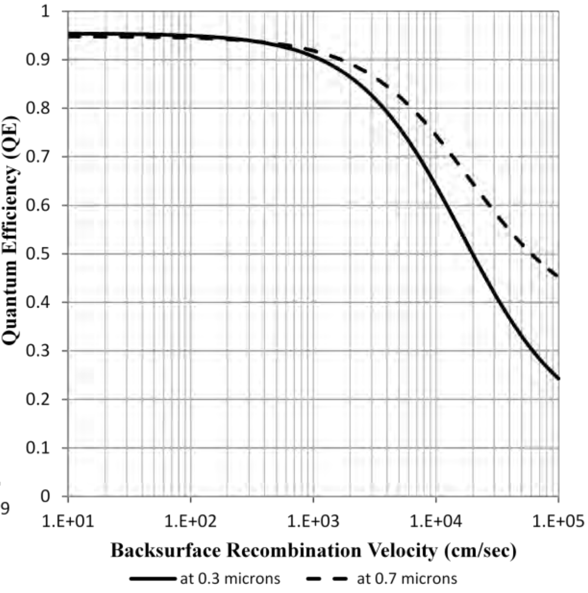

Figure 3. Dependence of quantum efficiency (QE) calculated at 0.3 microns and 0.7 microns versus back surface recombination velocity.

CURRENT VOLTAGE CHARACTERIC OF A SOLAR CELL

Dark currents from the n-side absorber layer should only limit high-quality DLH devices operating in the diffusion-limited region. In a proper design of a detector, the absorber layer thickness t_n is less than the diffusion length of the minority carriers. Current density of a solar cell under illumination is given by

$$J(V) = J_d(V) - J_{ph}(\emptyset, QE)$$

where $J_d(V)$ is the total dark current density of the solar cell and $J_{ph}(\emptyset, QE)$ is the photocurrent density under the illumination. V is the voltage drop between the cathode and anode, QE is the quantum efficiency, and ϕ is the incident flux in photons/cm^2/sec. This equation assumes zero series resistance and large shunt resistance compared to the zero bias resistance.

Under illuminated conditions, photo current density is given by

$$J_{ph}(\emptyset, QE) = q\int_0^{\lambda_c} QE(\lambda)\varphi d\lambda$$

where λ_c is the gap wavelength of CdTe. Here, the assumption is that all of the radiation up to the CdTe bandgap wavelength is absorbed in the CdTe layer and the wide-bandgap layer is a window to the below CdTe layer and acts as a passivant to reduce surface charges.

Total dark current density is the overall current density under no illumination and is given by

$$J_d(V) = J_{Diff} + J_{g-r} + J_{BTB} + J_{TAT} + J_{SH}$$

where J_{Diff} is the diffusion current density from the neutral regions of the junction, J_{g-r} is the g-r current density from the depletion region, and J_{BTB} and J_{TAT} are the tunneling current densities. The tunneling current densities come in two forms, namely, band-to-band (BTB) and trap-assisted tunneling (TAT), where forbidden gap energy states promote and participate in a two-step process BTB, TAT. J_{SH} is the shunt current density related to the surface states or through the junction.

VARIOUS CURRENT CONTRIBUTIONS OF A SOLAR CELL

Diffusion dark current density of a solar cell can be expressed as follows[12]:

$$J_{Diff} = J_{0Diff}\left[\exp\left(\frac{qV}{nkT}\right) - 1\right] \tag{2}$$

where q is the electron charge, k is Boltzmann's constant, T is absolute temperature, n is the ideality factor equals to 1, V is the voltage across the diode, and J_{oDiff} is the reverse saturation diffusion current density consisting of components from the p and n-sides of the junction, expressed here in current density superposition form as[12-15]

$$J_{0diff} = qn_i^2\left[\frac{L_p}{N_d\tau_p} + \frac{L_n}{N_a\tau_n}\right]$$

where J_{0diff} denotes diffusion current density, $L_{p,n}$ and $\tau_{p,n}$ denote minority diffusion lengths and lifetimes on respective n and p sides of the junction , and $N_{d,a}$ denote donor and acceptor concentration levels on the n and p sides of the junction. For the case of p-on-n double layer heterostructures, where the p-side has a wider bandgap and high doping N_a, the second term in J_{0diff} is negligible compared to the first and J_{0diff} reduces to

$$J_{0diff} = \frac{qn_i^2 L_p}{N_d\tau_p}$$

Minority-carrier lifetime in n-type CdTe is determined by several different recombination mechanisms, discussed extensively in the literature [40-53]. In particular, radiative and Shockley-Read-Hall (SRH) processes are important recombination mechanisms in CdTe and non-radiative Auger process at room temperature is not that important.

Radiative recombination lifetime has been described in terms of[16-18]

$$\tau_R = \frac{1}{B(n_0 + p_0)}$$

with B given by

$$B = 5.8\times10^{-13}\varepsilon^{1/2}\left(\frac{m_0}{m_e^* + m_h^*}\right)\left(1+\frac{m_0}{m_e^*}+\frac{m_0}{m_h^*}\right)\times\left(\frac{300}{T}\right)^{3/2}\left(E_g^2 + 3kTE_g + 3.75k^2T^2\right)$$

giving τ_R in seconds. ε is the dielectric constant, equal to be 10.6. Also, m_0 is the electron rest mass, m^*_e and m^*_h are the electron and hole effective masses. The recombination of electron-hole pairs occurs between conduction and valence bands, and the excess energy is released in the form of photons.

Finally, the Shockley-Read lifetime, assuming a single recombination level E_t below the conduction band edge, and low injection levels, has been described in terms of [19]

$$\tau_{SR} = \frac{\tau_{p0}(n_0 + n_1)}{n_0 + p_0} + \frac{\tau_{n0}(p_0 + p_1)}{n_0 + p_0},$$

where τ_{n0} and τ_{p0} denote shortest-time constant values for electron and hole capture, respectively, $n_1 = n_0 \exp(E_t - E_F)/kT$, $p_1 = p_0 \exp(E_F - E_t)/kT$, and E_F denotes the Fermi energy.

When the lifetime is not dominated by a single process, it is necessary to calculate the lifetime accordingly. Thus if all recombination mechanisms are important, the overall effective lifetime τ is then calculated from

$$\frac{1}{\tau} = \frac{1}{\tau_R} + \frac{1}{\tau_{SR}}$$

where τ_R and τ_{SR} are, radiative and SRH lifetimes, respectively.

Figure 5 shows the dependence of minority-carrier lifetime on majority electron density of n-type CdTe at 300 K. The solid line indicates the radiative lifetime and when doping is 10^{17} cm^{-3}, the lifetime values are in the low 100 nSec range. The dashed lines show the 100- and 500-nsec SRH contributions. Diffusion length of carriers can be calculated assuming hole mobility of 200 cm^2/Vs in n-type, as shown in the Fig 3. Diffusion lengths are greater than 5 microns for majority doping of less than 10^{17} cm^{-3} and this is sufficient to satisfy $t_n < L$ for complete absorption.

When the n-type active (absorber) layer thickness t_n is smaller than the diffusion length L_p, dimension t_n effectively replaces L_p to give

$$J_{odiff} = \frac{qn_i^2 t_n}{N_d \tau_p}$$

Diffusion current is seen to be proportional to n_i^2 and is the fundamental limitation of the dark current mechanisms of an optimized cell, where

$$n_i^2 = N_c N_v \exp\left(-\frac{E_g}{kT}\right)$$

where $N_{c,v}$ denotes the electron and hole densities, respectively, in the conduction, valence band; and E_g is the bandgap.

Another fundamental limitation arises from the depletion region and is known as generation-recombination currents from the depletion region. Early treatments developed the seminal formulation for generation-recombination phenomena in semiconductor junctions[20]. Phenomenologically, electron-hole pairs generated thermally in the depletion region give rise to recombination and generation currents under forward bias and reverse bias, respectively. Trap levels due to defects are most effective when they exist close to the intrinsic Fermi level, i.e., when $E_t = E_i$. With assumptions that $E_t = E_i$ and $\tau_{po} = \tau_{no} = \tau_o$, it follow under these provisos, $J_{g\text{-}r}$ reduces to[21]

$$J_{g-r} \approx \frac{\mathrm{n_i W_{dep} kT}}{2\tau_0}\left[\exp\left(\frac{\mathrm{qV}}{\mathrm{2kT}}\right)-1\right]$$

where W_{dep} is the depletion width. As can be seen from the above equation, generation-recombination J_{g-r} current density is seen to be proportional to n_i.

In all of the modeling discussed in poly-related CdTe solar cells in the literature, the g-r currents are significant and limit the overall performance of CdTe solar cells.

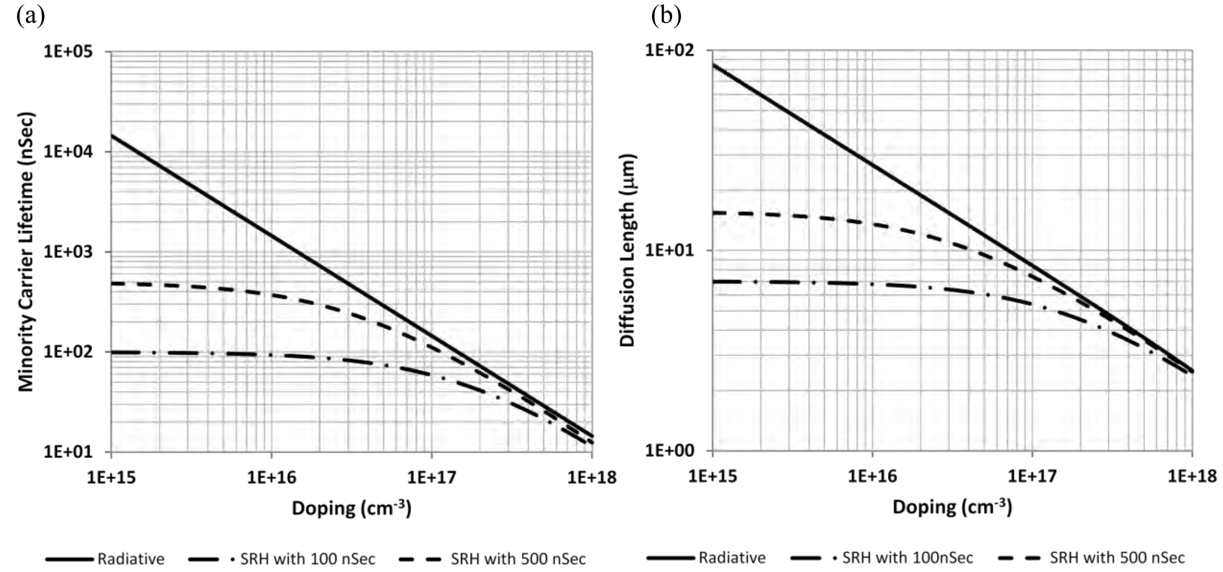

Figure 3. (a) Dependence of minority carrier lifetime on doping. Lines show various recombination mechanisms. Solid line is for radiative and dash lines with 100 nsec, 500 nsec SRH contribution in addition to the radiative recombination. (b) Calculated diffusion length versus doping. Calculation assumes 200 cm^2/Vse of hole mobility.

Tunneling currents can dominate under certain conditions especially at low temperatures, where thermally generated currents are low, and this is the dominant current mechanism under reverse biases. Tunneling currents come in two forms: (1) BTB and (2) TAT, where forbidden gap energy states promote and participate in a two-step process. BTB tunneling currents result in electrons tunneling directly from the valance band to the conduction band and are given by[13]

$$J_{BTB} = \frac{q^3 EV}{4\pi^2\hbar^2}\sqrt{\frac{2m^*}{E_g}} * \left[\exp\left(-\frac{4\sqrt{2m^*}E_g^{1.5}}{3qE\hbar}\right)\right] * \left[1-\exp\left(\frac{qV}{kT}\right)\right]$$

where E is the electric field, $\hbar$ is the reduced Planck constant, m^* is the tunneling effective mass, and E_g is the bandgap. These currents are due to direct tunnelling of carriers under relatively high reverse biases. Most probably, these currents, BTB and TAT in wide bandgap solar cell junctions, are insignificant.

TAT current (J_{TAT}) arises from electrons transitioning from the valence band to a trap level within the forbidden gap and then tunneling to the conduction band. The current density is given by[12]

$$J_{TAT} = \frac{\pi^2 q^2 m^* E M^2 N_t W}{\hbar^3 (E_g - E_t)}\sqrt{\frac{2m^*}{E_g}} * \left[\exp\left(-\frac{\sqrt{m^*/2}\,E_g^{1.5} F(a)}{2qE\hbar}\right)\right] * \left[1-\exp\left(\frac{qV}{kT}\right)\right]$$

where M is the transition matrix element, N_t is the trap density in cm^{-3}, E_t is the trap energy, and F(a) is a function of E_t/E_g. Finally, currents due to shunting (I_{SH}) across the diode are given by

$$J_{SH} = \frac{V}{A * R_{SH}}$$

where R_{SH} is the shunt resistance. Usually, surface leakage currents and shunt currents are due to the intersection of dislocation and defects which are possible sources of this category of excess currents.

The efficiency of a solar cell is given by

$$\eta = \frac{J_{sc} V_{oc} FF}{W}$$

where J_{sc} is the short-circuit current density, which is equal to the photo current density $J_{ph}(\phi, QE)$; V_{oc} is the open circuit voltage; FF is the fill factor; and W is the incident solar energy.

The open circuit voltage, V_{oc} is given by

$$V_{oc} = \frac{kT}{q} log_e \left[\frac{J_{ph}}{J_d} + 1\right]$$

From the above equation, for a high efficiency solar cell, J_{sc}, V_{oc}, and FF need to be maximized. Minimization of the dark current J_d is key to increasing the V_{oc}.

By substituting for optimum diffusion currents and V_{oc} reduces to

$$V_{oc} = \frac{E_g}{q} - \frac{kT}{q} log_e \left[\frac{q N_c N_v t_n}{J_{ph} N_d \tau}\right]$$

and, with dominant g-r currents, V_{oc} reduces to

$$V_{oc} = \frac{E_g}{q} - \frac{2kT}{q} log_e \left[\frac{q\sqrt{N_c N_v} W_{dep}}{2 J_{ph} \tau}\right]$$

Figure 4 shows V_{oc} versus CdTe n-type doping for diffusion limited dark currents (with recombination due to radiative and SRH) and g-r limited dark currents. As seen, radiative recombination gives the highest V_{oc}, which is 1.1 V. In addition, radiative recombination with SRH contribution (with 500 nsec and with 150 nsec) gives V_{oc} close to radiative values for doping higher than 10^{17} cm^{-3} in the CdTe base layer. Figure 4 shows that V_{oc} increases with doping up to 10^{17} cm^{-3} and saturates up to a doping level of 10^{18} cm^{-3}. However, beyond that doping level, V_{oc}falls off for the diffusion limited case. Hence, the optimum doping concentration is determined to be10^{17} cm^{-3}. This is a reasonable value for achieving an optimum diffusion length as well as ohmic contacts to the device. In the case of poly-CdTe solar cells, the reported maximum lifetime values are in the 2-nsec range with g-r dominant dark currents. In this case, the calculated V_{oc} is 0.77 to 0.90 V for doping concentrations between 10^{15} cm^{-3} to 10^{17} cm^{-3}. The calculation is in agreement with experimental obtained values reported in the literature. To summarize, this section, Figure 4 shows that V_{oc} can be increased with increased doping; this is a key factor in enhancing the efficiency of poly-CdTe-based solar technology. On the other hand, a SRH lifetime of 2 nsec under conditions of diffusion dark currents results in an increased V_{oc} compared with the g-r limited dark currents. This is about 13% increase in V_{oc} up to the doping of 10^{17} cm^{-3}.

Lastly, evaluating the overall efficiency of a solar cell (see Figure 5) along with different recombination values shows that an efficiency of 29% can be achieved with at a doping level of 10^{17} cm^{-3} with diffusion limited dark currents. Figure 5 also illustrates the efficiency of poly-CdTe solar cell versus doping. Based on these considerations, standard poly-CdTe with a lifetime of 2 nsec and g-r limited behavior results in a minimum efficiency of 15% (for doping of 10^{15} cm^{-3}) and a maximum of 19% (for doping of 10^{18} cm^{-3}), in contrast to the diffusion limited with 150-nsec lifetimes. Assumed input power from sunlight AM1.5 of $1000 W/m^2$.

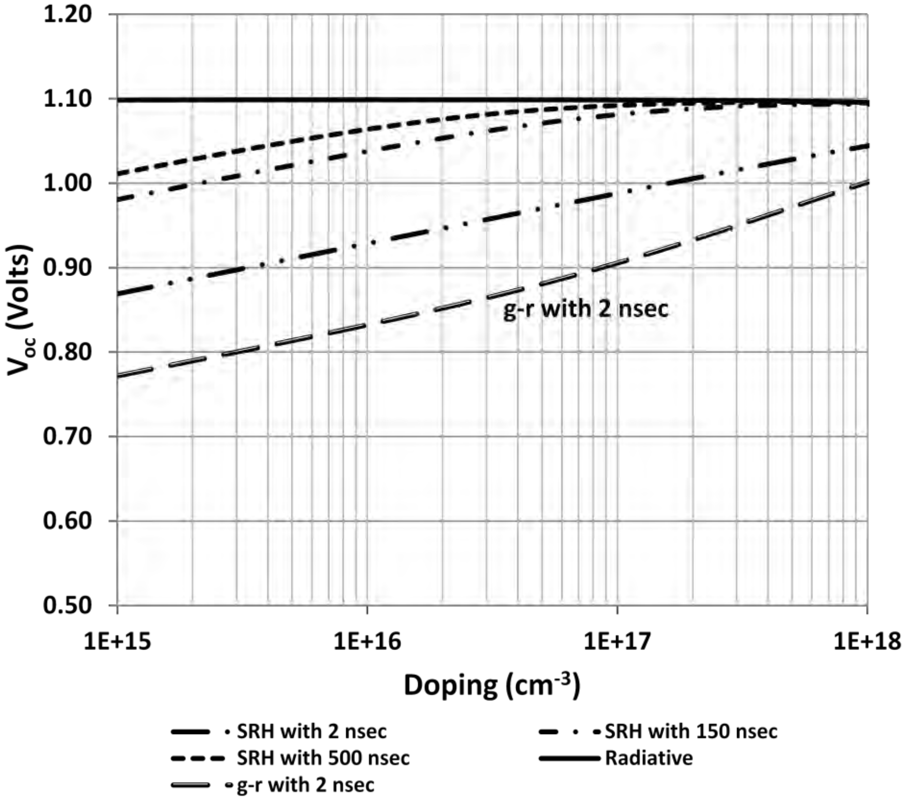

Figure 4. Dependence V_{oc} versus CdTe base layer doping. Lines show different recombination values/mechansims as indicated in the figure.

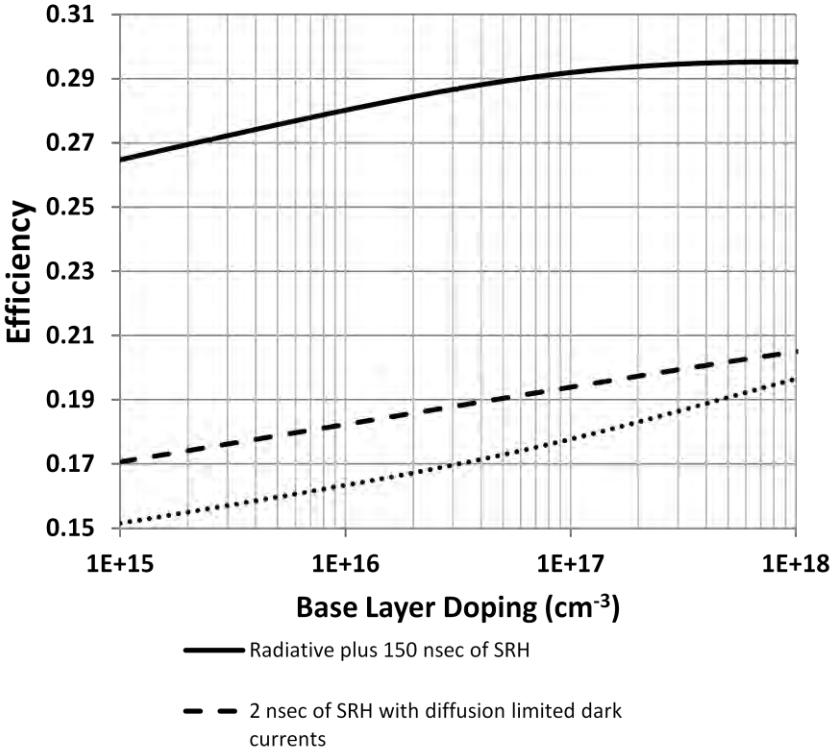

Figure 5. Calculated solar efficiencies versus CdTe base layer doping density. Lines show different recombination values/mechanisms as indicated in the figure.

CONCLUSIONS

The overall efficiency of CdTe solar cell has been calculated. Despite long-term research efforts on CdTe solar cells, measured CdTe solar cells efficiencies are far below theoretical limits. On the basis of the model presented here, the large difference between the measured and theoretical efficiencies can be minimized by considering crystalline CdTe material rather than poly-CdTe. The electrical as well as optical qualities of this poly-CdTe are limited due grain sizes/boundaries. Minority mobility and carrier lifetimes drastically affect the overall cell efficiency. Back surface recombination velocity is a critical parameter to maximize the QE in the entire wavelength range and should be less than 10^3 cm/sec. In the case of poly-CdTe, efficiency can be maximized by increasing doping. The model presented here was for backside illuminated conditions but could be used under front side illuminated conditions as well.

REFERENCES

1. Sivalingam Sivananthan, James W. Garland, and Michael W. Carmody, “Multijunction single-crystal CdTe-based solar cells: Opportunities and challenges,” Proc. of SPIE Vol. 7683, 76830N (2010).
2. Ramesh Dhere, Presentation at SPIE Orlando, FL, 2010.
3. S.M. Johnson, T.J. deLyon, C.A. Cockrum, W.J. Hamilton, T. Tung, F.I. Gesswein, B.A. Baumgratz, L.M. Ruzicka, O.K. Wu, and J.A. Roth, J. Electron. Mater. 24, 467, (1995).
4. J.M. Peterson, J.A. Franklin, M. Reddy, S.M. Johnson, E. Smith, W.A. Radford, and I. Kasai, J. Electron. Mater. 35, 1283, (2006).
5. Gregory Brill, Yuanping Chen, Priyalal Wijewarnasuriya, and Nibir Dhar, “Infrared Focal Plane Array Technology Utilizing HgCdTe/Si: Successes, Roadblocks, and Material Improvements,” Proc. of SPIE, Vol. 7419, 74190L, (2009).
6. Photovoltaic World - The Magazine for Solar Power, May/June 2011.
7. EPIR Technologies, Bolingbrook, IL.
8. P. S. Wijewarnasuriya, M. Zandian, D. D. Edwall, W. V. McLevige, C. A. Chen, J. G. Pasko, G. Hildebrandt, A. C. Chen, J. M. Arias,I. D’Souza, S. Rujirawat, and S. Sivananthan, “MBE P-on-n Hg1−xCdxTe heterostructure detectors on silicon substrates,” J. Electron. Mater., 27, 6, 546–549, (Jun. 1998).
9. W.W. Anderson, Infrared Phys. V20, 363, (1980); F. Urbach, Phys. Rev. 92, 1324, (1953); E. Finkman, S.E. Schacham, J. Appl. Phys. V56, 2896, (1984).
10. Harold J. Hovel, Semiconductors and Semimetals, Vol. 11 Solar Cells, Academic Press, Inc.
11. www.nrel.gov/docs/gen/fy04/36831.pdf#ovw. R.K. Ahrenkiel, “Electrical and Optical Characterization of Semiconductors,” DOE/National Association of State Universities and Land Grant Colleges (NASULGC) Biomass and Solar Energy Workshops, August 3-4, 2004.
12. B.G. Streetman, "Solid State Electronic Devices," 1980, Prentice-Hall, inc.Englewood Cliffs, NJ, 07632.
13. S.M. Sze, "Physics of Semiconductor Devices", Second Edition, Pg. 92, 1981, John Wiley & Sons, Inc. NY
14. W. Shockley, "Electrons and Holes in Semiconductors," D. Van Nostrand, Princeton, NJ, 1950.
15. Y. Nemirovsky, D. Rosenfeld, R. Adar, A. Kornfeld, J. Vac. Sci. Tech. A, 7, 528 (1989).
16. R.G. Pratt, J. Hewett, P. Capper, C.L. Jones, and M.J. Quelch, J. Appl. Phys. 54, 5122 (1983).
17. P.S. Wijewarnasuriya, M.D. Lange, S. Sivananthan, and J.P. Faurie, J. Appl. Phys. 75, 1005 (1994).
18. P.S. Wijewarnasuriya, M.D. Lange, S. Sivananthan, and J.P. Faurie, J. Elect. Mat. Vol. 24, 545 (1995).
19. J.S. Blakemore, Semiconductor Statistics, Pergamon, NY, 1962.
20. M.B. Reine, T.J. Tredwell, A.K. Sood, “Photovoltaic Infrared Detectors,” Semiconductors and Semimetals 18, R.K. Willardson and A.C. Beer editors, Academic Press, NY, 1981.
21. Sheng S. Li, Semiconductor Physical Electronics, Plenum Press, NY, 1993.
22. M.A. Kinch, J. Vac. Sci. technol. 21, 215 (1982).

NO. OF COPIES	ORGANIZATION
1 ELEC	ADMNSTR DEFNS TECHL INFO CTR ATTN DTIC OCP 8725 JOHN J KINGMAN RD STE 0944 FT BELVOIR VA 22060-6218
39	US ARMY RSRCH LAB ATTN IMNE ALC HRR MAIL & RECORDS MGMT ATTN RDRL CIO LL TECHL LIB ATTN RDRL CIO MT TECHL PUB ATTN RDRL SEE A RUGEL-EVANS ATTN RDRL SEE D SEELEY ATTN RDRL SEE E SYVRUD ATTN RDRL SEE G SIMONIS ATTN RDRL SEE G WOOD ATTN RDRL SEE I F SEMENDY ATTN RDRL SEE I G BRILL ATTN RDRL SEE I G SUN ATTN RDRL SEE I H HIER ATTN RDRL SEE I J LITTLE ATTN RDRL SEE I K K CHOI ATTN RDRL SEE I K OLVER ATTN RDRL SEE I K SABLON-RAMESEY ATTN RDRL SEE I N DHAR ATTN RDRL SEE I P FOLKES ATTN RDRL SEE I P TAYLOR ATTN RDRL SEE I P UPPAL ATTN RDRL SEE I P WIJEWARNASURIYA (10 HCS) ATTN RDRL SEE I S SVENSSON ATTN RDRL SEE I U LEE ATTN RDRL SEE I W BECK ATTN RDRL SEE I W SARNEY ATTN RDRL SEE I Y CHEN ATTN RDRL SEE J ELLER ATTN RDRL SEE K MAJOR ATTN RDRL SEE L BLISS ATTN RDRL SEE P GILLESPIE ADELPHI MD 20783-1197